TriDes – a new tool for the design, development and non-destructive evaluation of advanced construction steels

R. Nevshupa[a]✉, E. Roman[b], K.E. Grinkevych[c], I. Martinez[a]

a. Institute of Construction Sciences "Eduardo Torroja" (IETCC-CSIC), Spanish National Research Council, (Madrid, Spain)
b. Institute of Material Sciences of Madrid (ICMM-CSIC), Spanish National Research Council (Madrid, Spain)
c. Frantsevich Institute for Problems of Materials Science of NASU (Kiev, Ukraine)
✉r.nevshupa@csic.es

ABSTRACT: Design and development of advanced steel types require establishing an optimal combination of mechanical strength, resistance to hydrogen degradation and durability, among others; however, the available tools for assessing some of these properties are limited. A novel tool for supporting the design and development of steel types was therefore created. This tool, called TriDes, is based on the phenomenon of mechanically stimulated gas emission and allows for determining mechanical properties and hydrogen concentration locally, with high spatial resolution and during different phases of the service life of construction steel elements. Its applicability to the development of pipe steel with improved durability, as well as to steel types used in marine environments, has been investigated.

KEYWORDS: Steel; Mechanical properties; Physical properties; Characterization; Microstructure

RESUMEN: *TriDes – una nueva herramienta para el diseño, desarrollo y evaluación no destructiva de aceros avanzados de construcción.* El diseño y desarrollo de acero avanzado requiere establecer una combinación óptima de resistencia mecánica, resistencia a la degradación por hidrógeno y la durabilidad, entre otras. Sin embargo, las herramientas disponibles para evaluar experimentalmente algunas de estas propiedades son limitadas. Por lo tanto se creó una nueva herramienta, llamada TriDes. Esta técnica está basada en un principio físico distinto de los que se usan en las técnicas establecidas y combina la caracterización de hidrógeno en el acero en y la caracterización mecánica y/o tribológica. La técnica es portatil lo que permite determinar concentración local de hidrógeno con alta resolución espacial durante todo el ciclo de vida de elementos fabricados en acero y además evaluar la dureza y resistencia al desgaste del acero. Se ha investigado la capacidad de la técnica para el desarrollo de aceros para aplicaciones en gasoductos y construcciones marinas.

PALABRAS CLAVE: Acero; Propiedades mecánicas; Propiedades físicas; Caracterización; Microestructura

1. INTRODUCTION

The accumulation of hydrogen in construction steel types is of great concern for structural health, since hydrogen can harmfully affect the mechanical properties of metallic constructions that are in contact with aggressive environments through hydrogen embrittlement, stress corrosion cracking and corrosion fatigue (1, 2). For high-strength steel types used in bridge construction, e.g., wires for the

post-tensioning of bridges and the pre-stressing of suspension cables, an increase in local hydrogen concentration to a threshold level may result in delayed cracking at stress levels below the yield strength, as well as the loss of ductility (3, 4). In some cases, wires can be protected from hydrogen embrittlement through the application of zinc coatings, although controversial results have also been reported indicating that zinc in contact with alkaline cement can enhance hydrogen generation (5, 6). Furthermore, the susceptibility of ferritic stainless steel types used for metallic construction to hydrogen embrittlement – especially in marine environments – is a primary drawback that impedes the replacement of austenitic stainless steel types by cheaper and higher strength ferritic types (7). Similar problems exist for other metallic alloys (8, 9).

During the past several decades, a number of researchers have sought to determine the relationship between the composition (7), microstructure (10, 11), residual stress (12), environment (8) and susceptibility of metallic alloys to hydrogen degradation in order to obtain a "critical mass" of knowledge, necessary for optimal design and development of advanced construction steel types that have specific properties for particular applications. Considering that local hydrogen concentration in metallic alloys cannot generally be measured during experiments due to the lack of a simple, reliable, cheap and non-destructive technique suitable for being used in any laboratory, various standard procedures have been adopted to normalize experimental conditions, thereby enabling the comparison of results from various studies involving hydrogen degradation of steel types, e.g., the ammonium-thiocyannate test for checking susceptibility to stress-corrosion cracking (13). This significantly limits flexibility in the selection of the most effective tools for designing and developing new construction steel types. Thus, hydrogen absorption and diffusion in stressed metallic alloys generally involves a simulation approach or modelling experiments (14, 15). Only a few studies have investigated the correlation between hydrogen local concentration and hydrogen damage of construction steel types using neutron radiographic imaging (16), neutron diffraction (17), nuclear resonance reaction analysis (17) and secondary ion mass-spectrometry (SIMS) (18).

All of the above techniques require large or singular installations with high-energy ion and neutron beams. Even when these techniques are available, the alloy under study must preferably be subjected to stress and aggressive media *in situ* or immediately prior to characterization, due to the high diffusivity and fugacity of hydrogen, i.e. in conditions that are different from the real ones. All of these issues significantly hamper the research and effective use of such techniques in the design of materials.

On the other hand, there is a need for the early diagnosing of hydrogen damage in metallic constructions (19). The problem exists because obtained information about the susceptibility of alloys to hydrogen degradation consist of general characteristics that cannot be used for the prediction of the behaviour of a specific construction, since many parameters that control hydrogen absorption are unknown or have not been well-determined in terms of service life. It is worth mentioning that investigating different monitoring techniques for hydrogen damage effected to construction steel types is among the priorities of governmental administrations in various countries (20, 21).

The aim of this work is to present a novel technique for hydrogen characterization in construction steel types that is based on the physical principle of mechanically stimulated gas emission (22). This technique, known as TriDes, has several advantages compared to other conventional methods that make it a powerful tool in the design and development of advanced construction steel, and for use in the macroscopically non-destructive evaluation of real-life constructions (23).

2. METHODOLOGY AND EXPERIMENTAL APPARATUS

2.1. Mechanically stimulated gas emission as a novel phenomenological basis for the technique (TriDes) applied to hydrogen characterization in construction metallic alloys

Mechanically stimulated gas emission (MSGE) is a phenomenon consisting of the emission of gases from the surface and bulk of a solid or surface coating under any type of mechanical action including scratching, rubbing, indentation, etc. For metallic alloys, hydrogen is generally the primary emitted gas, whereas traces of methane, carbon mono- and dioxide, as well as water vapours among others can also be detected (24, 25). By doping metals with deuterium, it was shown that mechanically stimulated hydrogen emission is associated with hydrogen being dissolved and occluded in the bulk of the metal (26). In addition, hydrogen emission can in part be the result of the decomposition of metal hydrides (27).

A previous study has shown that under certain experimental conditions, the emission of hydrogen from the bulk of metallic alloys is a non-thermally driven process, associated with plastic deformation and fracture rather than with frictional heating (28). Though the exact physicochemical mechanisms responsible for MSGE are not clear, this phenomenon can be associated with transport of H atoms bonded to moving dislocations, stimulation of hydrogen diffusion by stress gradients, etc. Therefore, the amount of emitted hydrogen is generally a function of two

parameters: the deformed volume of the metallic alloy and the average concentration of hydrogen in this volume. This concept has been proven in various experiments using nickel, iron, carbon and stainless steel (22, 29, 30), and has further been theoretically developed by the Nevshupa group (22–24).

According to this concept, the amount of hydrogen emitted due to mechanical action, N_{td}, can be determined from the following expression (28) [1]:

$$N_{td} = k_{td} \int_{t_0}^{t_1} C_H(t) \frac{dV}{dt} dt ,$$ [1]

where t_0 is the time of the beginning of mechanical action, t_1 is the time of the end of mechanical action, k_{td} is the calibration coefficient, dV is the volume of new material involved in the mechanically affected zone in the time interval dt and C_H is the local hydrogen concentration in the volume of the material dV.

On the other hand, N_{td} can be experimentally determined by integration of the pressure time series (26, 31) [2]:

$$N_{td} = S \int_{t_0}^{t_f} \Delta p(t) \, dt ,$$ [2]

where S is the pumping speed that is constant for the given experimental system, $\Delta p = p(t) - p_b$ is the pressure increase in a vacuum chamber due to MSGE, p_b is the equilibrium background pressure and t_f is the time when pressure returns to p_b.

A typical pressure time series obtained in the experiments with high-strength, low-alloy carbon steel is shown in Figure 1. Graph I was measured for an as received steel sample, with a hydrogen mass concentration below 1.1 ppm, whereas graph II was acquired for a steel sample following corrosion. Variables 1 and 2 are explained in the figure.
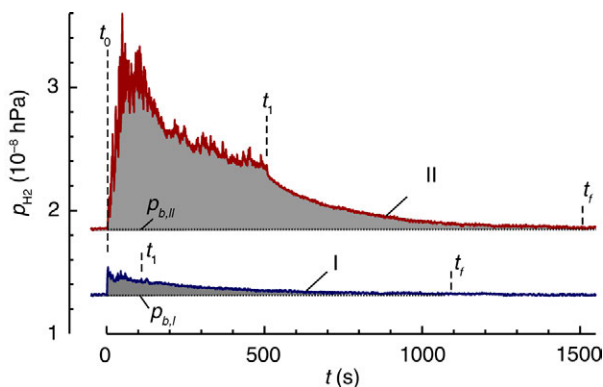

FIGURE 1. Pressure time series during rubbing of high-strength low-alloy steel grade R4 [47]: I – as received, II – following corrosion test. Duration of mechanical action was 100 s for I and 500 s for II. Shaded areas correspond to the integral indicated in (2).

In many cases, retarded hydrogen emission occurred for tens of minutes following the end of mechanical action. Retarded emission is evidence of the non-thermal character of the driving forces of MSGE and can be associated with slow processes of hydrogen diffusion, recombination and desorption. Thus, analysis of the kinetics of retarded emission can provide a deeper understanding of these processes, since it can provide additional information about gas-solid reactions, which is essential for the effective design of advanced steel types. Moreover, the use of mass-spectrometry offers the possibility for characterizing the emission of other gases. By examining the tribodesorption of methane and other hydrocarbons the chemical reactions between hydrogen and carbonaceous phases, i.e. graphite, cementite, etc., can be better understood (32, 33).

Integration in [2] must include the retarded gas emission; therefore, t_f is generally much larger than t_1.

For simplicity, it can be considered that hydrogen concentration does not vary in the tested strata of the material. Then, by combining [1] and [2], the average concentration of hydrogen can be found from the following expression [3]:

$$C_H = S \frac{\int_{t_0}^{t_f} \Delta p(t) dt}{\int_{t_0}^{t_1} \frac{dV}{dt} dt} .$$ [3]

The integral in the denominator in [3] is the volume of the material that contributes to gas emission, i.e., MSGE active material that can be assumed as being approximately equal to the volume of the mechanically affected zone (MAZ), V_d.

It should be noted that quantification of MSGE active material is not an easy task. Measurement of the geometry of MAZ allows for estimating the "apparent" volume of the MAZ, i.e., the volume of displaced or worn material. The zones surrounding the MAZ can also contribute to hydrogen emission due to diffusion. This is evidenced by retarded emission tails that can last for thousands of seconds following the mechanical action. For the sake of simplicity and the applicability of the method in practice, it is suggested that the volume of MSGE active material be estimated from the "apparent" volume of the MAZ, V_a, by introducing a calibration coefficient, k_{td} [4]:

$$V_d = k_{td} V_a ,$$ [4]

This suggestion is based on the assumption that for the same material and under similar loading and rubbing conditions, the ratio of the volume of MSGE active material to the "apparent" volume of the MAZ is nearly constant. The physical meaning of the calibration coefficient is the ratio of the volume

of MSGE active material to the "apparent" volume of the MAZ under given experimental conditions and for given material. The calibration coefficient can be determined by a comparison of the experimental results found by TriDes and those obtained by a reference technique, e.g., SIMS, neutron- and ion beam techniques among others, in a reference sample, or by using standard samples for which gas content is known. Bearing in mind the high fugacity of dissolved hydrogen in metals, quasi-stable light metal hydrides such as MgH_2 can serve as a reference material. The benefits of using quasi-stable metal hydrides include a constant and well-defined hydrogen concentration that strictly corresponds to the compound stoichiometry, fast and complete dehydration during MSGE and fast emission of H_2 from the residual α-Mg phase (27). Calibration must be carried out under similar loading conditions, test duration and using an indenter of the same geometry.

When the calibration coefficient is not known, tests can be used for the semi-quantitative study of the relative increase of gas concentration after various treatments or on different parts of the sample, while always maintaining the same loading conditions. For a true quantitative measurement of the gas concentration, TriDes should be calibrated against an established method that can provide a reliable reference.

The "apparent" volume of the MAZ can be experimentally measured using stylus profilometry, optical confocal microscopy or another technique suitable for the determination of the 3D geometry of the mechanically affected zone.

Figure 2a shows the reconstructed 3D geometry of the MAZ on the surface of an as received high-strength low-alloy steel sample. Three cross-section profiles of the mechanically affected zone measured at various y coordinates are shown in Figure 2b. For mechanical action, the material was scratched by a hard conical tip made of tungsten carbide.

Once cross-section profiles of MAZ $z=f(x)$ have been measured, V_a can be found by integration of z in the space domain [5]:

$$V_a = l \int_{x_0}^{x_1} f(x)\,dx , \qquad [5]$$

where l is the length of the MAZ and x_0 and x_1 are the coordinates of the sides of the mechanically affected zone (Figure 2b).

To reduce measurement uncertainty, x_0 and x_1 can be defined as the coordinates of the intersection of the profile, with the horizontal line corresponding to the initial surface.

For the example shown in Figure 2b, the shaded cross-section area is 160 μm^2, which yields the average volume of the MAZ as approximately 10^{-3} mm^3 (with l=7 mm). The depth of the analysis ranged from 4 μm to 6.7 μm. For deeper penetration into
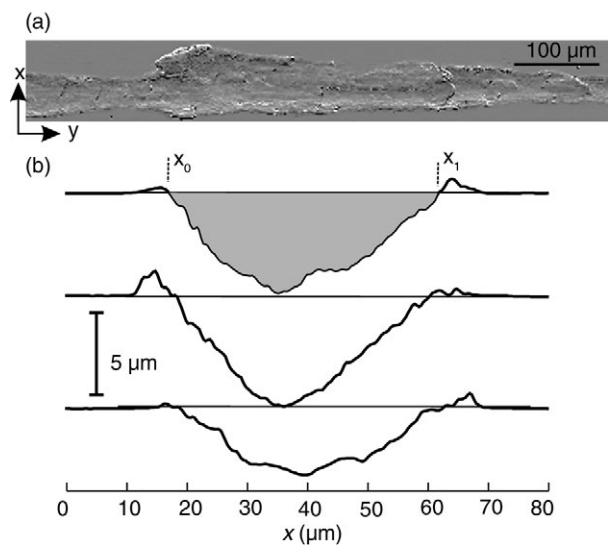

FIGURE 2. Geometry of the mechanically affected zone following the MSGE test for the as received high-strength low-alloy sample; a) portion of a reconstructed image obtained by confocal optical microscopy; b) three cross-section profiles of the mechanically affected zone. Shaded area corresponds to the integral of the MAZ cross-section profile.

material, a higher load or larger number of rubbing cycles can be used.

These results evidence the significant benefits of the developed method compared to conventional approaches. These advantages are especially notable when compared with the widely used hot-extraction technique (HET). Although the ultimate detection limit of TriDes is not yet as high as for HET, TriDes offers excellent depth and lateral resolution that is unachievable by HET. Additionally, TriDes is relatively simple, does not require strong electric and magnetic fields or high-energy ion and neutron beams; therefore, it can be employed as a habitual laboratory technique. Table 1 summarizes the main characteristics of TriDes and other methods.

Another important advantage of TriDes is that it is naturally combined with mechanical and/or tribological characterization, e.g., indentation and scratch test among others, which can provide valuable complimentary information pertaining to hardness, plastic properties, etc. Combination these two techniques shows promise for the future development of a complex and macroscopically non-destructive evaluation method for construction steels (35).

2.2. Apparatus for hydrogen characterization in the construction of metallic alloys using the TriDes method

Figure 3 shows a schematic drawing of the experimental apparatus developed for the characterization of construction materials using the TriDes method (36).

TABLE 1. Typical characteristics of various techniques for the analysis of hydrogen content in solids

Technique	Detection limit	Resolution	
		depth	lateral
Elastic recoil detection analysis	0.1 at.%	2–5 nm	20 μm
Dynamic secondary ion mass-spectrometry	ppb – ppm	2–30 nm	50 nm–30 μm
Neutron reflectometry	1 at.%	1 nm	10 μm
Small angle neutron scattering		<10 nm	1–300 nm
Glowing discharge optical emission spectrometry	ppm	10 nm	4 mm
Electron energy loss spectrometry	< 2 at.%		1 nm
Nuclear resonance reaction analysis	0.5 at.%	< 1 nm	1 mm
Hot extraction technique (HET)	ppb	–	–[1]
TriDes	< 1 ppm	< 40 nm	< 100 μm

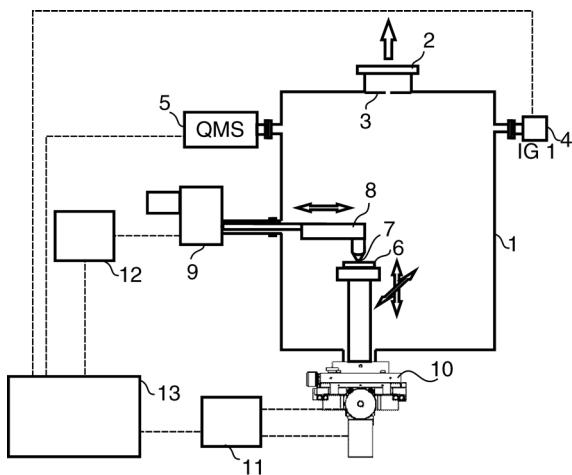[1] For ppb resolution, the required amount of material is roughly 100 g (34).

FIGURE 3. Schematic drawing of the experimental apparatus developed for the characterization of construction materials using the TriDes method: 1 – vacuum chamber; 2 – pumping line; 3 –diaphragm; 4 –ion gauge for gas pressure measurement; 5 – quadrupole mass-spectrometer; 6 – sample of the material; 7 –hard indenter; 8 – force gauges; 9 –motor for reciprocating motion of the indenter; 10 – x-y stage for sample displacement; 11, 12 – motors drives; 13 –computer for motion control and data acquisition.

The apparatus consists of vacuum chamber 1, pumped by corresponding vacuum pumps through a diaphragm 3. The diaphragm – with well-determined gas conductance – is necessary to control pumping speed S of the system, which is one of the parameters required for the determination of C_H (3). The composition of the emitted gases is measured by quadrupole mass-spectrometer 5. Sample 6, mounted on motorized vacuum-tight x-y linear stage 10, is rubbed by hard indenter 7. The indenter can perform reciprocating motion using linear motor 9. The applied normal load and the resulting friction force are measured by force gauges 8. The motion of the linear motor and the x-y stage is controlled by drives 11 and 12 and computer 13, which is also used for the acquisition of signals from the ion gauge, QMS and force gauges.

The apparatus allows for controlling the following experimental parameters: normal load, sliding velocity, pass length of the indenter and the number of rubbing cycles. In a previous study, the pumping speed for hydrogen S=27.4 l/s was experimentally determined (37).

To establish optimal experimental parameters, one must consider various aspects including material hardness, expected hydrogen concentration, the presence of surface layers (23), etc. For example, a larger number of rubbing cycles must be used for metals with higher hydrogen content and for samples with surface oxide layers. For softer materials, a smaller number of rubbing cycles and rounded-shape indenters is recommended.

3. CASE STUDIES

3.1. Application of the TriDes method for the design and development of steel types for gas main pipes

Low carbon ferrite-perlite steel types are widely used for primary gas and oil pipes due to the combination of high strength, high toughness and deformability that are critically important in severe environments, seismic regions, etc. However, during their service life, these steel types suffer from gradual deterioration that is characterized by a decrease in brittle-fracture resistance, impact strength and hardness and relative elongation, but an increase in uniform elongation (38). Steel degradation is usually attributed to microstructural changes resulting from non-stationary loading conditions and hydrogen absorption from the corrosive environment and transported oil and gas. Comparative studies have shown that steel from pipes in service had higher efficiency for hydrogen trapping, as well as a larger number and depth of hydrogen traps than steel from buffer stock pipes. This was manifested by decreasing

the apparent hydrogen diffusivity and permeability in steel during the course of service life (39).

These requirements, which are low cost and have good weldability and manufacturability, are generally met by the following two steel types: API5L-X52 and 17G1S (GOST 19282 analogous to DIN 1.0570). These steel types belong to the same class and have very similar chemical compositions (Table 2). However, little is known about the relationship between their microstructure, mechanical properties and resistance to hydrogen degradation. To study these relationships, we applied the TriDes technique.

Microstructure analysis (Figure 4) was carried out following standard metallographic procedures. The polished specimens were etched with a 4% nital solution. The microstructure of X52 steel was generally uniform with equiaxial polygonal grains, although certain band elongation was observed. Steel 17G1S had a more dispersed acicular ferrite-perlite structure with massive ferrite regions, as well as granular ferrite and bainitic ferrite with high density dislocation and second phases in the matrix (40).

Mechanical characteristics of the samples: Vickers hardness, HV, tensile strength, σ, area reduction, ψ, relative elongation, δ and Charpy impact energy, K_{CV}, are summarized in Table 3. In addition, tribological characterization was carried out in a normal atmosphere and in lubricated conditions in two modes using the procedure previously described (41). A hard steel ball 8 mm in diameter was used as indenter. The frequency of reciprocating motion was 0.5 Hz, friction stroke 8 mm and sliding velocity 0.013 m/s. In the first mode, a constant normal load 30 N was applied, while in the second dynamic mode, in addition to a constant load, a sinusoidal component with amplitude 3 N was applied in the normal direction.

The comparison of friction forces F_I and F_{II} and the wear characteristics obtained for these two modes provide insight into the capability of the material to dissipate supplied mechanical energy via plastic deformation and fracture (35, 42). Steel 17G1S had slightly higher strength, plasticity and impact toughness, than steel X52. Additionally, it showed a higher capacity to resist wear under dynamic loading.

TriDes experiments were carried out under reciprocating rubbing of steel samples by a spherical indenter made of alumina and 3 mm in diameter. The applied normal load was 1.7 N, mean sliding speed was 0.2 m/s, motion frequency was 1 back-and-forth stroke per second and stroke length was 7 mm. The tests were repeated for each sample, varying the number of rubbing cycles, n. After the tests were completed, the geometry of the MAZs was studied using an optical confocal microscope. The apparent volume of the deformed material as a function of n was determined as a product of mean cross-section area and stroke length, and is shown in Figure 5.

X52 steel suffered significantly more severe damage than 17G1S. Figure 6 shows the cross-section

TABLE 2.   Nominal chemical composition of X52 and 17G1S steel types

	C	Mn	Si	S	P	Cu	Ni	Cr	Mo
X52	0.16	1.60	0.15–0.50	0.007	0.025	0.30	0.30	0.25	0.08
17G1S	0.15–0.2	1.15–1.6	0.15–0.2	<0.04	<0.035	<0.3	<0.03	<0.03	

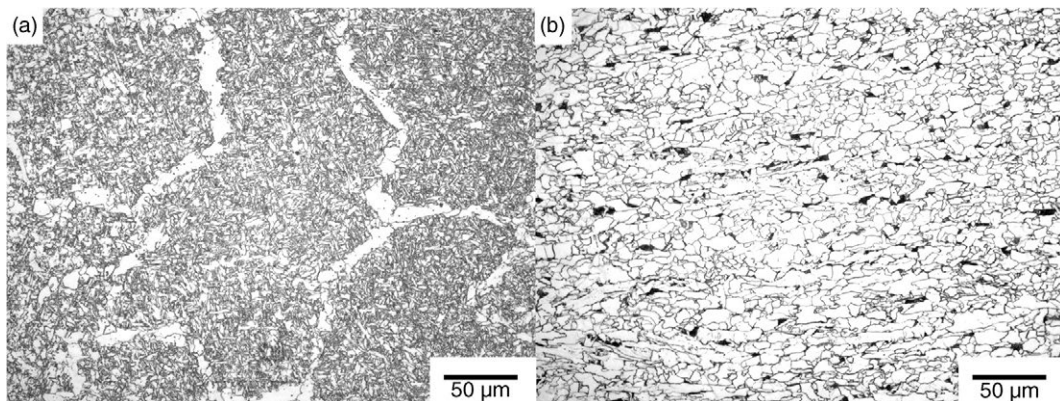|	V	Nb	Ti	Sn	B	As	N	Al
X52	0.06	0.04	0.02	0.02	0.0005		0.014	<0.06
17G1S						<0.08	0.008	

FIGURE 4.   Microstructures of steel types: a) 17G1S; b) X52. White zones = ferrite; grey zones = perlite.

TABLE 3. Mechanical and tribological characteristics of the samples

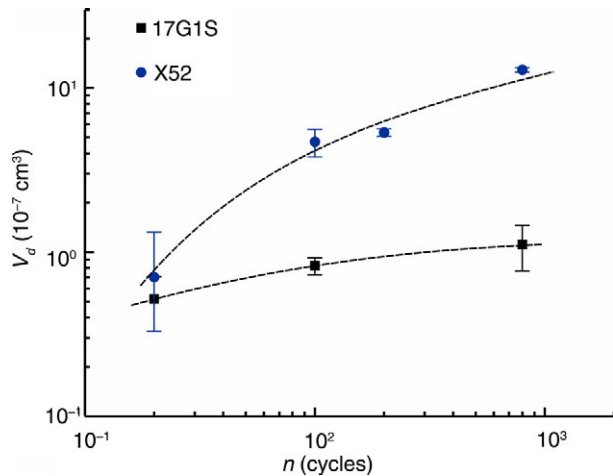|	HV, GPa	σ, MPa	ψ, %	δ	K_{CV}, J	F_I, N	F_{II}, N
X52	1.83	475	72.9	22.7	177	14.5	3.9
17G1S	1.85	595	79	22.9	206	9.8	0.9

FIGURE 5. Apparent volume of deformed material as a function of the number of rubbing cycles. The experimental data with standard errors are shown by dots.

profiles for these two steel types after 800 rubbing cycles. For 17G1S, the deformed zone could hardly be distinguished from surface roughness, whereas for X52, a deep and regular mark, which conformed with the spherical indenter, was found. In both cases, deformation was plastic, which can be inferred from edging on the sides of the MAZ; however, for 17G1S, this was much less intensive than for X52.

It should be noted that the volume of MSGE active material, schematically shown by the hatched area in Figure 6b, is larger than the "apparent" volume represented by the grey shaded area. Since under similar experimental conditions and for similar materials the ratio of the "apparent" volume of the MAZ to the volume of MSGE active material is nearly constant, relative variations of hydrogen concentrations in these two very similar steels can be assessed by considering only the "apparent" volume of the MAZ [6]:

$$\frac{C_{H,1}}{C_{H,2}} = \frac{\int_{t_{01}}^{t_{f1}} \Delta p_1(t)\,dt}{\int_{t_{02}}^{t_{f2}} \Delta p_2(t)\,dt} \frac{V_{a,2}}{V_{a,1}}, \qquad [6]$$

where subscripts 1 and 2 correspond to the first and the second steel, respectively.

The amount of hydrogen emitted from these steel types under rubbing as a function of the rubbing cycles are shown in Figure 7. It should be noted that

each dot corresponds to a different test. Generally, the amount of hydrogen increased alongside the number of rubbing cycles. For X52, the rate of the increase was approximately three-fold higher than for 17G1S. This can be associated with the higher extent of plastic deformation in the case of X52. In some cases, the behaviour of hydrogen emission was not uniform, as can be seen for X52. This can be attributed to irregular wear behaviour, which depends on many factors including surface inhomogeneity and variation of the loading conditions. However, from a comparison of the data in Figs. 5 and 7, a fairly good correlation between the amount of hydrogen and the deformed volume was found.

In fact, when N_{td} is plotted as a function of V_a, near linear behaviour but with different slopes can be observed (Figure 8). Deviation from the trend at higher V_a can be related to an underestimation of the volume of MSGE active material at higher loads and longer rubbing duration. Although for steel 17G1S the total amount of emitted hydrogen was smaller than for X52, the slope of the fitted linear graph was higher. This finding suggests that hydrogen concentration in the analysed surface layer of 17G1S had to be almost one order of magnitude larger than in X52.

From our previous studies, we determined that the calibration coefficient for such steel types can be in the range 16±4; thus, the estimated true hydrogen concentration should be roughly 4.2×10^{-4} mol/cm^3 for 17G1S and 4.5×10^{-5} mol/cm^3 for X52. These values are somewhat higher than those in the literature obtained via electrolytic measurements (43); this can be attributed to the higher extraction capacity of TriDes. In fact, mechanical activation has shown to be capable of promoting hydrogen desorption even from strongly bonded states (27), whereas hydrogen from deep traps could not be fully extracted using the electrolytic technique. It should also be stressed that our results corresponded to a thin surface layer of about one micrometre in depth, where hydrogen concentration is usually up to one order of magnitude higher than in the bulk (17, 44, 45). For a more precise estimation of hydrogen concentration, the calibration coefficient should be more precisely determined for the experimental conditions in question. A higher concentration of hydrogen in 17G1S can be associated with a more dispersive microstructure and larger interface areas between ferrite and cementite, which can offer a larger number of hydrogen traps. These findings are in line with previous studies (38).
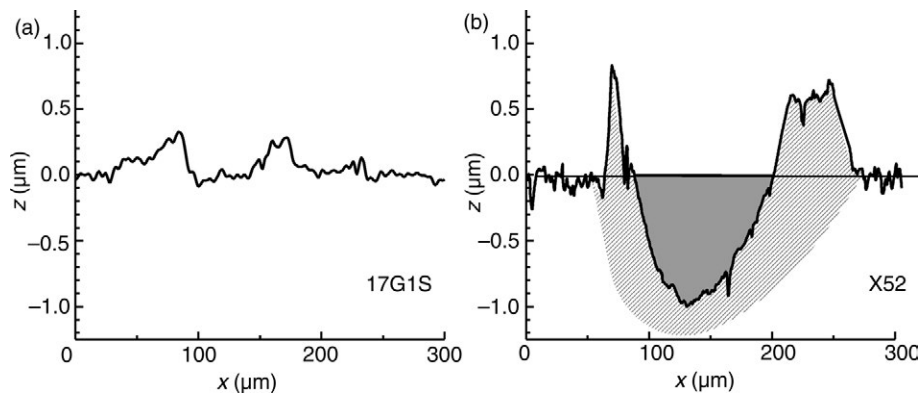
FIGURE 6. Cross-section profiles of the MAZ after 800 rubbing cycles for a) 17G1S steel; b) X52 steel. Apparent deformed volume is shown in grey, while real deformed volume is schematically shown by the hatched area.
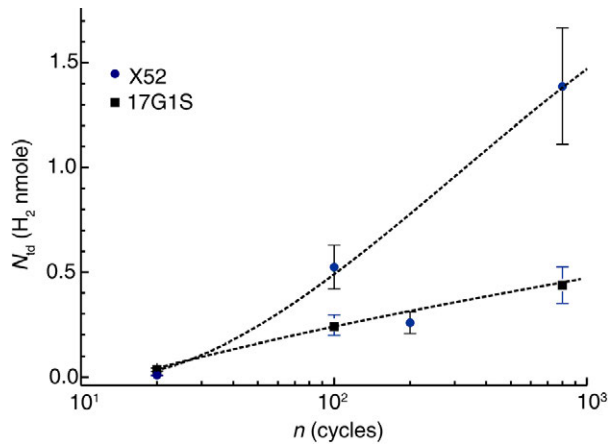

FIGURE 7. Amount of hydrogen emitted from the steel types as a function of the number of rubbing cycles. The dots represent the experimental data. The error bars show confidence intervals for sample means at significance level 0.05.
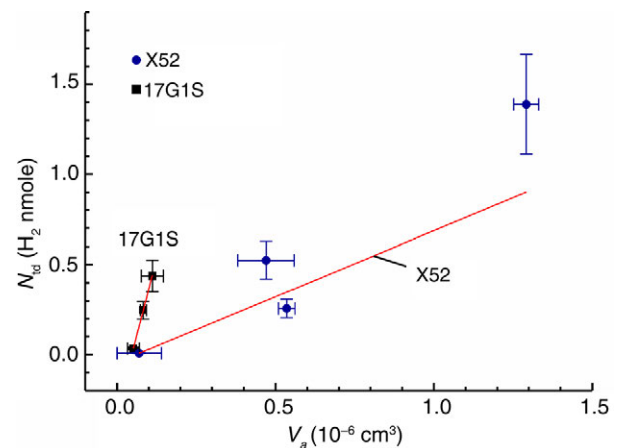

FIGURE 8. Amount of emitted hydrogen as a function of the apparent deformed volume. Lines are mean-square linear fits of the experimental data. The error bars show confidence intervals for sample means at significance level 0.05.

Analysis of the retarded emission showed that the time constants of the decay for 17G1S and X52 were very similar: 377 ± 32 s and 317 ± 143 s, correspondingly. This result may indicate that the basic physical and chemical mechanisms behind hydrogen emission from both steel types are the same, and are likely related to hydrogen diffusion in ferrite, followed by recombination desorption from the surface (26).

Possible reactions between hydrogen and carbon were analysed through the characterization of methane emission. The average ratio of the total amounts of emitted methane to hydrogen was in the range of 0.5% to 1.4% for X52, but only 0.06% to 0.57% for 17G1S. Such a notable difference can be interpreted in terms of surface tribochemical reactions, the rate of which depends on the contact area rather than the volume of mechanically activated bulk material (see Figure 6). These findings also indicated that X52 can be more susceptible to hydrogen-assisted carbon migration, which has

been suggested as one of the main reasons for in-service degradation. Although these steel types are not susceptible to hydrogen embrittlement, their fracture toughness is extremely sensitive to microscopic structural faults. Generation of these faults was associated with the enhancement of carbon diffusion by hydrogen. Previous studies evidenced a pronounced correlation between the decrease in fracture toughness and an increase in hydrogen content (46). However, our study suggests that's that although it is an important factor, taken alone, hydrogen concentration cannot be a criterion of steel degradation. Hydrogen concentration must be considered jointly with steel microstructure. In fact, previous research has shown that X52 steel suffered more intensively during service degradation than 17G1S under similar service conditions (41). These results can be helpful in designing and developing more durable steel types and in optimizing technological processes.

3.2. Comparative study of hydrogen absorption in ferrite-perlite and martensitic construction steel types under corrosion in sea water

The corrosion process is one of the main reasons for increasing hydrogen concentration in construction steel; however, little is known about the effect of microstructures on absorption capability and the distribution of hydrogen in bulk of steels. Therefore, this case study focuses on the characterization of relative hydrogen concentration in two types of construction steel subjected to free corrosion in synthetic seawater. The steel types were B500SD, which is used in construction, as well as high-strength low alloy steel grade R4, used in offshore mooring (47). The microstructures of these steel types are shown in Figure 9. B500SD had a regular ferrite-perlite structure with equiaxial polygonal ferrite grains, while R4 had a typical, tempered martensite structure.

The samples were rectangular sheets, 13×80 mm^2 and 4 mm thick. Prior to conducting tests, the samples were ground and degreased in an ultrasonic bath using acetone and isopropanol. B500SD was immersed without protective coatings, whereas R4 was protected from contact with water by a polymeric coating, with the exception of a 2 cm^2 window area on one side of the sample. Experimental conditions during immersion in synthetic seawater, prepared in accordance with ASTM D1141, were the following: temperature in the range of 24 °C to 26 °C and atmospheric pressure 907 hPa to 914 hPa. B500Sd was corroded under saturated oxygen concentration, whereas for R4, oxygen concentration was kept at 1 ± 0.15 mg/l. Hydrogen was characterized in as received and corroded samples. For R4, hydrogen was characterized on both the corroded and non-corroded (back) surfaces. An alumina ball, 3 mm in diameter, was used as indenter for the softer B500SD, whereas a tungsten carbide cone tip was used for the harder R4. Alumina has been shown to yield insignificant gas emission (37, 48). In addition

to high wear resistance and high hardness, it has high thermal conductivity, thus reducing frictional heating.

Figure 10a and b (plot i) indicate the pressure time series obtained for as received samples B500SD and R4, respectively. There are notable differences pertaining to hydrogen emission behaviours between the two steel types. For B500SD, emission began with a sharp peak and gradually decreased to a nearly steady state pressure. For as received R4, the rate of hydrogen emission was much lower and almost uniform from the start of the test, with a slowly decreasing trend. The lower emission for R4 can be linked to vacuum degassing during smelting, whereas differences in behaviour should be associated primarily with microstructure. Subjecting B500SD to corrosion (Figure 10b) had only a scaling effect (at a nearly forty-fold increase), while the general shape of the graph did not change significantly. However, for R4 subjected to corrosion, both emission intensity and behaviour changed. The emission initially slowly rose and reached the maximum after 300 to 500 rubbing cycles. Once the rubbing ended, a notable leap was observed, which was followed by a long-term retarded emission. The leap indicated the existence of two emission modes, which have been discussed elsewhere (23). Increasing the test duration from 1000 to 2500 cycles (plots ii and iii in Figure 10c, correspondingly) did not result in any dramatic changes in emission behaviour. Surprisingly, the test performed on the non-corroded back surface of the R4 sample revealed significant increase in H$_2$ (Figure 10d). The general shape of the plot resembled that for B500SD (Figure 10b), although at a much lower intensity and with a more significant leap at t_1. After reaching the maximum at 100 to 200 cycles, emission rate steeply decreased.

The intensive peak at the start of rubbing for both steel types can be associated with high hydrogen concentration in the topmost surface layers.
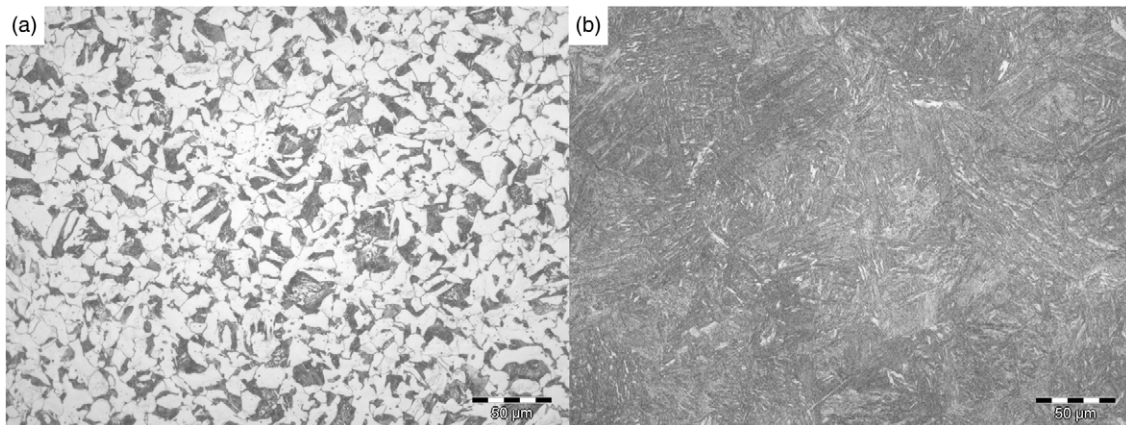

FIGURE 9.   Microstructures of two steels: a) ferrite perlite of B500SD (white = ferrite, grey = perlite); b) tempered martensite of R4.
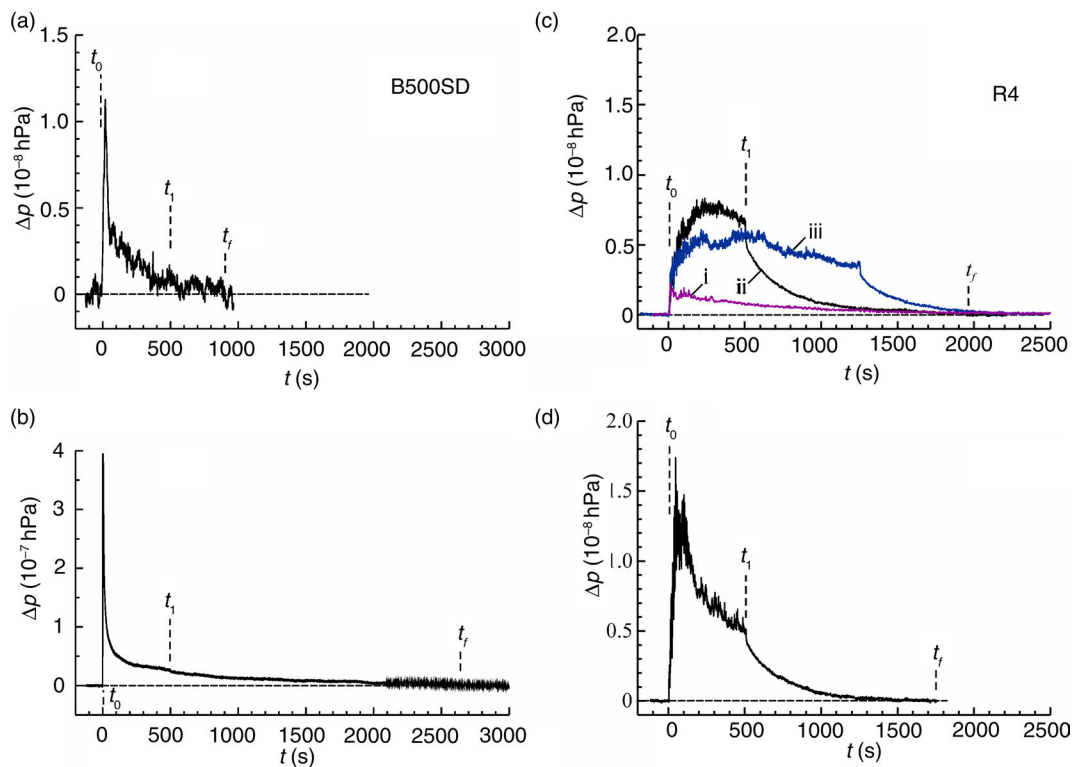
FIGURE 10.   Pressure (H$_2$) time series obtained during TriDes tests for steel samples: a) B500SD as received; b) B500SD after corrosion in seawater (note the different scale of the y axis; c) R4 as received (i) and after corrosion in seawater (exposed surface): ii = 1000 cycles, iii = 2500 cycles; d) R4 back surface not subjected to corrosion after corrosion test – 1000 cycles. Plots i and ii on panel (c) correspond to the tests with 1000 and 2500 rubbing cycles, respectively.

Previous research has shown that H concentration in a subsurface layer at a depth between 100 nm and 5 μm can be one to two orders of magnitude higher than the concentration of hydrogen in the bulk (17, 44, 45). It is suggested that higher hydrogen concentration is associated with defects generated during mechanical processing of the samples. The reason for the lack of such a peak on the corroded surface of R4 is not yet clear. On the one hand, it may be related to microstructural changes induced by corrosion, which led to the disappearance of hydrogen traps due to oxidation of the defect-rich layer. On the other hand, the presence of oxide particles can alter wear conditions, promoting more intensive abrasion (23). Further structural investigations are needed to clarify this phenomenon. A hydrogen increase on the side of the sample that was not exposed to seawater indicates that hydrogen absorption was significant even under free corrosion, i.e., without cathodic protection, as well as under reduced oxygen concentration.

It can be concluded that steel with large ferrite grains (B500SD) tend to absorb much larger amounts of hydrogen than martensitic steel. However, the presence of a dispersed carbide phase in martensite was not generally an obstacle for hydrogen diffusion in the steel samples.

Our findings question the appropriateness of the costly vacuum degassing of high-strength steel during fabrication if at a later stage, this steel will be used in marine and other aggressive environments without protective coatings. In practice, the smelting of steel intended for use in bridges, mooring systems and in other crucial applications is generally subjected to various steps of vacuum degassing, until hydrogen concentration drops below a certain established value, normally 1.2 ppm. However, as demonstrated in this study, when steel components are exposed to corrosive environments, hydrogen concentration spontaneously increases several-fold, even in the absence of factors accelerating hydrogen absorption such as stress and cathodic protection, among others. Generally, the steel types did not suffer from hydrogen degradation under such conditions. This work invites further investigation into the influence of residual hydrogen on the performance, durability and reliability of construction materials, and where TriDes can serve as a powerful tool for the characterization of local hydrogen concentration. Furthermore, it is suggested that discussion be initiated concerning possible reconsideration of acceptable levels of residual hydrogen concentration in high-strength construction steel types.

4. CONCLUSIONS

The results of this study demonstrate the advanced features of the novel TriDes method and its applicability in the design, development and macroscopically non-destructive evaluation of construction steels. These features include: local analysis using only a thousandth part of a cubic millimetre of material; space- and depth-resolved analysis; simultaneous characterization of hydrogen emission and mechanical properties; analysis of other gases in order to comprehend synergism between hydrogen and carbon in steel types. The possibility to characterize different zones of the same sample in order to study hydrogen distribution and diffusion in steel subjected to corrosion was demonstrated. TriDes has been used in the design and development of more durable pipe steel that is less susceptible to microstructural degradation. These studies will be continued in the future and involve steel characterization using TriDes as a means for establishing the duration of service life. Analysis of hydrogen absorption during the corrosion of high-strength low-alloy (HSLA) steel demonstrated a considerable increase in hydrogen concentration even without cathodic protection. Hydrogen had high mobility in HSLA steel, despite the presence of barriers of dispersed carbides. These results suggest establishing a dialogue towards the possible reconsideration of the appropriateness of the established limits for hydrogen concentrations in steel used for offshore applications.

ACKNOWLEDGEMENTS

REFERENCES

1. Robertson, I.; Sofronis, P.; Nagao, A.; Martin, M.L.; Wang, S.; Gross, D.W.; Nygren, K.E. (2015) Hydrogen Embrittlement Understood. *Metall. Mater. Trans. A* 46 [6], 2323–2341. http://dx.doi.org/10.1007/s11661-015-2836-1.
2. Hirth, J. (1980) Effects of hydrogen on the properties of iron and steel. *Metall. Trans. A* 11 [6], 861–890. http://dx.doi.org/10.1007/BF02654700.
3. Ćwiek, J. (2009) Hydrogen degradation of high-strength steels. *J. Achievments Mater. Manuf. Eng.* 37, 193–212.
4. Nakamura, S.-i.; Suzumura, K. (2009) Hydrogen embrittlement and corrosion fatigue of corroded bridge wires. *J. Constr. Steel Res.* 65 [2], 269–277. http://dx.doi.org/10.1016/j.jcsr.2008.03.022.
5. Ettouney, M.M.; Alampalli, S. (2011) Infrastructure Health in Civil Engineering: Applications and Management, Boca Raton, CRC Press. http://dx.doi.org/10.1201/b11174.
6. Ganz, H.R. (2012) Effect of zinc on prestressing steel, Lausanne, FIB.
7. Kim, S.; Chun, Y.; Won, S.; Kim, Y.; Lee, C. (2013) Hydrogen Embrittlement Behavior of 430 and 445NF Ferritic Stainless Steels. *Metall. Mater. Trans. A* 44 [3], 1331–1339. http://dx.doi.org/10.1007/s11661-012-1265-7.
8. Jin, S.; Gayle, N.V.; Chen, C.T.; Lichamer, J.R.; Ghilarducci, C. (1980) Humidity-induced hydrogen embrittlement in an Fe-Cr-Co magnet alloy. *Metall. Trans. A* 11 [5], 854–856. http://dx.doi.org/10.1007/BF02661218.
9. Bond, G.M.; Robertson, I.M.; Birnbaum, H.K. (1988) Effects of hydrogen on deformation and fracture processes in high-ourity aluminium. *Acta Metall.* 36 [8], 2193–2197. http://dx.doi.org/10.1016/0001-6160(88)90320-3.
10. Michler, T.; Naumann, J. (2010) Microstructural aspects upon hydrogen environment embrittlement of various bcc steels. *Int. J. Hydrogen Energy* 35 [2], 821–832. http://dx.doi.org/10.1016/j.ijhydene.2009.10.092.
11. Wang, M.; Tasan, C.C.; Koyama, M.; Ponge, D.; Raabe, D. (2015) Enhancing Hydrogen Embrittlement Resistance of Lath Martensite by Introducing Nano-Films of Interlath Austenite. *Metall. Mater. Trans. A* 46 [9], 3797–3802. http://dx.doi.org/10.1007/s11661-015-3009-y.
12. Elices, M.; Ruiz, J.; Atienza, J.M. (2004) Influence of residual stresses on hydrogen embrittlement of cold drawn wires. *Mater. Struct.* 37 [5], 305–310. http://dx.doi.org/10.1007/BF02481676.
13. Toribio, J.; Kharin, V. (2006) Effect of residual stress-strain profiles on hydrogen-induced fracture of prestressing steel wires. *Mater. Sci.* 42 [2], 263–271. http://dx.doi.org/10.1007/s11003-006-0079-4.
14. Sanchez, J.; Fullea, J.; Andrade, C.; de Andres, P.L. (2008) Hydrogen in alpha -iron: Stress and diffusion. *Phys. Rev. B* 78 [1], 014113. http://dx.doi.org/10.1103/PhysRevB.78.014113.
15. Palma Carrasco, J.; Silva Diniz, D.; Andrade Barbosa, J.M.; Almeida Silva, A. (2012) Numerical modeling of hydrogen diffusion in structural steels under cathodic overprotection and its effects on fatigue crack propagation. *Materialwiss. Werkstofftech.* 43 [5], 392–398. http://dx.doi.org/10.1002/mawe.201200971.
16. Berger, H.; Polichar, R.; Rowe, W.J. (1987) *Corrosion Detection by Real-Time Neutron Imaging*, in *Neutron Radiography*, J. Barton, et al., Editors. Springer Netherlands. p. 563–570. http://dx.doi.org/10.1007/978-94-009-3871-7_69.
17. Castellote, M.; Fullea, J.; de Viedma, P.G.; Andrade, C.; Alonso, C.; Llorente, I.; Turrillas, X.; Campo, J.; Schweitzer, J.S.; Spillane, T.; Livingston, R.A.; Rolfs, C.; Becker, H.W. (2007) Hydrogen embrittlement of high-strength steel submitted to slow strain rate testing studied by nuclear resonance reaction analysis and neutron diffraction. *Nucl. Instrum. Methods Phys. Res., Sect. B* 259 [2], 975–983. http://dx.doi.org/10.1016/j.nimb.2007.03.084.
18. Awane, T.; Fukushima, Y.; Matsuo, T.; Matsuoka, S.; Murakami, Y.; Miwa, S. (2011) Highly Sensitive Detection of Net Hydrogen Charged into Austenitic Stainless Steel with Secondary Ion Mass Spectrometry. *Anal. Chem.* 83 [7], 2667–2676. http://dx.doi.org/10.1021/ac103100b.
19. Mil'man, Y.; Nykyforchyn, H.; Hrinkevych, K.; Tsyrul'nyk, O.; Tkachenko, I.; Voloshyn, V.; Mordel, L. (2012) Assessment of the In-Service Degradation of Pipeline Steel by Destructive and Nondestructive Methods. *Mater. Sci.* 47 [5], 583–589. http://dx.doi.org/10.1007/s11003-012-9431-z.
20. Virmani, Y.P.; Clemena, G.G. (1998) Corrosion protection - concrete bridges, U.S: Department of Transportation, Federal Highway Administration, McLean, Virginia.
21. Spencer, B.F.; Ruiz-Sandoval, M.E.; Kurata, N. (2004) Smart sensing technology: opportunities and challenges. *Struct. Control Health Monit.* 11 [4], 349–368. http://dx.doi.org/10.1002/stc.48.
22. Nevshupa, R.; Roman, E.; Konovalov, P.; de Segovia, J.L. (2008) New method to determine gas content in materials. *J. Phys.: Conf. Ser.* 100, 072030. http://dx.doi.org/10.1088/1742-6596/100/7/072030.
23. Nevshupa, R.; Cruz, K.; Martinez, I.; Ramos, S.; Llorente, I.; Roman, E. (2016) Triboemission of gases from iron and construction steel: The effect of surface conditions.

Tribol. Int. 97, 360–370. http://dx.doi.org/10.1016/j.triboint.2016.01.051.

24. Nevshupa, R.A.; Roman, E.; de Segovia, J.L. (2013) Contamination of vacuum environment due to gas emission stimulated by friction. *Tribol. Int.* 59, 23–29. http://dx.doi.org/10.1016/j.triboint.2012.07.009.

25. Řepa, P. (1992) Mechanically induced desorption. *Vacuum* 43 [5–7], 367–371. http://dx.doi.org/10.1016/0042-207X(92)90039-Y.

26. Nevshupa, R.A.; Roman, E.; de Segovia, J.L. (2008) Origin of hydrogen desorption during friction of stainless steel by alumina in ultrahigh vacuum. *J. Vac. Sci. Technol. A* 26 [5], 1218–1223. http://dx.doi.org/10.1116/1.2968682.

27. Nevshupa, R.; Ares, J.R.; Fernández, J.F.; del Campo, A.; Roman, E. (2015) Tribochemical Decomposition of Light Ionic Hydrides at Room Temperature. *J. Phys. Chem. Lett.* 6 [14], 2780–2785. http://dx.doi.org/10.1021/acs.jpclett.5b00998.

28. Nevshupa, R.A.; Roman, E.; de Segovia, J.L. (2010) Model of the effect of local frictional heating on the tribodesorbed gases from metals in ultra-high vacuum. *Int. J. Mater. Prod. Technol.* 38 [1], 57–65. http://dx.doi.org/10.1504/ijmpt.2010.031895.

29. Nevshupa, R. (2009) The role of athermal mechanisms in the activation of tribodesorption and triboluminisence in miniature and lightly loaded friction units. *J. Frict. Wear* 30 [2], 118–126. http://dx.doi.org/10.3103/s1068366609020081.

30. Frisch, B.; Thiele, W.-r. (1984) The tribologically induced effect of hydrogen effusion and penetration in steels. *Wear* 95 [2], 213–227. http://dx.doi.org/10.1016/0043-1648(84)90119-4.

31. Peressadko, A.G.; Nevshupa, R.A.; Deulin, E.A. (2002) Mechanically stimulated outgassing from ball bearings in vacuum. *Vacuum* 64 [3–4], 451–456. http://dx.doi.org/10.1016/S0042-207X(01)00335-9.

32. Rusanov, A.; Nevshupa, R.; Fontaine, J.; Martin, J.-M.; Le Mogne, T.; Elinson, V.; Lyamin, A.; Roman, E. (2015) Probing the tribochemical degradation of hydrogenated amorphous carbon using mechanically stimulated gas emission spectroscopy. *Carbon* 81, 788–799. http://dx.doi.org/10.1016/j.carbon.2014.10.026.

33. Rusanov, A.; Nevshupa, R.; Martin, J.-M.; Garrido, M.Á.; Roman, E. (2015) Tribochemistry of hydrogenated amorphous carbon through analysis of Mechanically Stimulated Gas Emission. *Diamond Relat. Mater.* 55, 32–40. http://dx.doi.org/10.1016/j.diamond.2015.02.007.

34. Merzlikin, S.V.; Mingers, A.M.; Kurz, D.; Hassel, A.W. (2014) An electrochemical calibration unit for hydrogen analysers. *Talanta* 125, 257–264. http://dx.doi.org/10.1016/j.talanta.2014.02.008.

35. Grinkevich, K. (2003) Some postulates of the structural dynamic concept of the tribosystem and their practical implementation. *J. Frict. Wear* 24 [3], 344–350. http://www.nasb.gov.by/eng/publications/trenie/tre24_3.php.

36. Roman, E.; Nevshupa, R.; de Segovia, J.L.; Konovalov, P.I.; Menshikov, I.P. (2007) Method and apparatus for analysis of gas content in solids and surface coatings. Patent WO2007ES70216 20071220, 23.02.2007

37. Nevchoupa, R.A.; De Segovia, J.L.; Deulin, E.A. (1999) An UHV system to study gassing and outgassing of metals under friction. *Vacuum* 52 [1–2], 73–81. http://dx.doi.org/10.1016/S0042-207X(98)00209-7.

38. Gabetta, G.; Nykyforchyn, H.M.; Lunarska, E.; Zonta, P.P.; Tsyrulnyk, O.T.; Nikiforov, K.; Hredil, M.I.; Petryna, D.Y.; Vuherer, T. (2008) In-service degradation of gas trunk pipeline X52 steel. *Mater. Sci.* 44 [1], 104–119. http://dx.doi.org/10.1007/s11003-008-9049-3.

39. Bockris, J.O.M.; Subramanyan, P.K. (1971) Hydrogen Embrittlement and Hydrogen Traps. *J. Electrochem. Soc.* 118 [7], 1114–1119. http://dx.doi.org/10.1149/1.2408257.

40. Zuo, X.; Zhou, Z. (2015) Study of Pipeline Steels with Acicular Ferrite Microstructure and Ferrite-bainite Dual-phase Microstructure. *Mater. Res.* 18, 36–41. http://dx.doi.org/10.1590/1516-1439.256813.

41. Tsyrul'nyk, O.T.; Nykyforchyn, H.M.; Zvirko, O.I.; Petryna, D.Y. (2004) Embrittlement of the steel of an oil-trunk pipeline. *Mater. Sci.* 40 [2], 302–304. http://dx.doi.org/10.1007/s11003-005-0018-9.

42. Mil'man, Y.V.; Grinkevich, K.E.; Mordel, L.V. (2014) Energy concept of hardness for instrumented indentation. *Russ. Metall. (Metally)* 2014 [4], 256–262. http://dx.doi.org/10.1134/S0036029514040089.

43. Capelle, J.; Dmytrakh, I.; Azari, Z.; Pluvinage, G. (2013) Evaluation of electrochemical hydrogen absorption in welded pipe with steel API X52. *Int. J. Hydrogen Energy* 38 [33], 14356–14363. http://dx.doi.org/10.1016/j.ijhydene.2013.08.118.

44. Deulin, E.A.; Nevshupa, R.A. (1999) Deuterium penetration into the bulk of a steel ball of a ball bearing due to its rotation in vacuum. *Appl. Surf. Sci.* 144–145, 283–286. http://dx.doi.org/10.1016/s0169-4332(98)00811-3.

45. Deulin, E.A.; Goncharov, S.A.; de Segovia, J.L.; Nevshupa, R.A. (2000) Mechanically stimulated solution of adsorbed hydrogen and deuterium in steel. *Surf. Interface Anal.* 30 [1], 635–637. http://dx.doi.org/10.1002/1096-9918(200008)30:1<635::AID-SIA855>3.0.CO;2-W.

46. Nykyforchyn, H.; Lunarska, E.; Tsyrulnyk, O.T.; Nikiforov, K.; Genarro, M.E.; Gabetta, G. (2010) Environmentally assisted "in-bulk" steel degradation of long term service gas trunkline. *Eng. Failure Anal.* 17 [3], 624–632. http://dx.doi.org/10.1016/j.engfailanal.2009.04.007.

47. Det Norske Veritas AS (2013) Offshore mooring chain. Standard DNV-OS-E302.

48. Nevshupa, R.A.; de Segovia, J.L.; Deulin, E.A. (1999) Outgassing of stainless steel during sliding friction in ultrahigh vacuum. *Vacuum* 53 [1–2], 295–298. http://dx.doi.org/10.1016/S0042-207X(98)00366-2.